International Journal of Fluid Machinery and Systems
Vol. 4, No.1, January-March 2011

DOI: 10.5293/IJFMS.2011.4.1.025
ISSN (Online): 1882-9554

Original Paper

Numerical Study of Inlet and Impeller Flow Structures in Centrifugal Pump at Design and Off-design Points

Kean Wee Cheah, Thong See Lee and Winoto S.H

Department of Mechanical Engineering, National University of Singapore
9 Engineering Drive 1, Block EA, 07-08, Singapore 117576
g0500401@nus.edu.sg, mpeleets@nus.edu.sg, mpewinot@nus.edu.sg

Abstract

The objective of present work is to use numerical simulation to investigate the complex three-dimensional and secondary flow structures developed at the inlet and impeller in a centrifugal pump at design and off-design points. The pump impeller is shrouded with 6 backward swept blades and with a specific speed of 0.8574. The characteristic of the pump is measured experimentally with straight and curved intake sections. Numerical computation is carried out to investigate the pump inlet flow structures and subsequently the flow field within the centrifugal pump. The numerical results showed that strong interaction between the impeller eye and intake section. Secondary flow structure occurs upstream at the pump inlet has great influence on the pump performance and flow structure within the impeller.

Keywords: centrifugal pump, impeller, inlet flow structure, secondary flow

1. Introduction

Centrifugal pumps are widely used in industrial and residential applications. These pumps vary in size, speed, characteristics and materials they are made of. Their fundamental role is to move liquid through a fluid system and to raise the pressure of the liquid. However, the inlet element of the pump come in different forms and shapes to achieve optimum inlet configuration. For example, an end suction pump normally comes with a flanged straight intake section while a vertical-in-line pump is fitted with a curved intake section. This is because each type of inlet configuration serves different purposes.

Predin and Biluŝ [1]'s experimental study on the inflow of a radial impeller pump found that the whirl flow or pre-rotation flow at the pump entrance pipe changed its direction of rotation because of the pre-rotation direction change around the impeller that caused by the different inlet angles of flow. Depending on the flow rate, the pre-rotation flow could be followed or opposed of the direction of impeller rotation. Bolpaire et al [2] further confirmed that the recirculation flow at impeller inlet at various flow rate by using the LDV measurement. In addition, Kikuyama et al [3] measured the static pressure changes on the impeller due to the interaction of the vortex caused by inlet swirl. The spiralling asymmetric vortex core induced by swirling flow will caused large unsteady pressure changes on the blade surfaces. Hence, the impeller is subjected to a large fluctuation of the radial force when there is a negative swirl flow.

The flow field inside a centrifugal pump is known to be strongly turbulent, three-dimensional and unsteady with recirculation flows at its inlet and exit, flow separation, and so on. One of the well known flow phenomenon within the radial flow impeller is the "jet wake" flow pattern developed near impeller exit. The flow separation in a centrifugal impeller normally occurs on the suction surface after the leading edge and forms a wake flow on the suction side. Bwalya and Johnson [4]'s experimental measurement on a centrifugal pump impeller at peak efficiency revealed that flow separation on the shroud/pressure corner at leading edge and travelled downstream axially through the impeller to form a wake in shroud/suction corner. At the impeller exit, a reversed radial velocity was observed due to high blade sweep angle. However, Howard and Kittmer [5] experimentally showed a low flow region occurred at suction tip corner. The measurements by Murakami et al [6] and Hong et al [7] showed that jet wake flow pattern is flow rate dependent and location of wake zone can changed significantly at impeller exit.

The flow field inside the impeller at off-design condition is also very different from design point. As reported by Pedersen et al [8], the smooth flow within the impeller at design point changed to a stalled flow at off-design design point. A large recirculation cell blocked the inlet to the stalled passage while a strong relative eddy dominated the remaining parts of the same passage and causing backflow along the blade pressure side at large radii. Liu et al [9] experimentally observed that the flow separation occurred on the curvature of blades at off-design condition as well. Due to decrease of flow rate, radial flow decelerated on shroud/suction surface, the secondary flow and vorticity increases in the passage. Further investigation by Abramian and Howard [10] using laser Doppler

Received October 13 2010; accepted for publication November 29 2010: Review conducted by Prof. Shuhong Liu. (Paper number O10024C)
Corresponding author: Kean Wee Cheah, Professor, g0500401@nus.edu.sg

anemometer measurement showed that pressure side mean flow separation under low flow condition within the impeller passage is affected by a combined effect between a secondary vorticity initiated at the inlet and a potential vortex which dominates the flow at impeller exit. The flow within the passage of the highly backward swept blades also dominated by the rotational effect because of the changing Rossby number along the curvature of the blade from the leading edge to trailing edge.

As the flow from the impeller is discharged into the non-symmetrical spiral volute casing, which sometimes can be fitted with a vaned diffuser, the strong interaction between the impeller and diffuser or spiral casing is expected. Dong et al [11] and Chu et al [12] used PIV measuring the velocity within the volute of a centrifugal pump at different impeller blade orientations, on and off-design conditions to study effect of impeller/volute tongue interaction. They found that jet-wake structures and pulsating flow near impeller exit. The orientation of the blades could affect the leakage and the pressure distribution. A vortex train generated as a result of non-uniform outfluxes from the impeller.

The objective of present work is to use numerical simulation to investigate the complex three-dimensional and secondary flow field developed at the inlet and impeller in a centrifugal pump at design and off-design point. First, the numerical simulation will study on how the inflow structure influences the flow field within the impeller passages. Second, the numerical simulation is to capture the dynamic and unsteady strong impeller volute casing interaction when flow exit from impeller at different operating points. At last, the investigation will study the unsteady flow structures that leaving the volute casing as well.

2. Experimental set up

The centrifugal pump used in this study consists of an impeller shrouded with six backswept blades, a curved intake section and a spiral volute casing. For straight intake section pump, the curved intake section is replaced with a straight pipe section. The specific speed, n_s of the centrifugal pump is 0.8574 and with a Reynolds number of 10^7 based on the impeller outer diameter and blade tip speed. The impeller inlet diameter d_1, and outlet diameter, d_2 is 202 mm and 356 mm respectively. The impeller outlet width, b_2 is 46.8 mm. The flow from impeller is discharged into a spiral volute casing with mean circle diameter d_3 of 374 mm. The impeller is designed to operate at 1450 rpm with a flow coefficient, ϕ of 0.0244 and head coefficient, ψ of 0.1033 at best efficiency point.

The experimental work is carried out according to the commonly adopted industrial test standard. The centrifugal pump test stand is an open test loop that designed for pumps to be tested in accordance to ISO 9906 Rotodynamic pumps – Hydraulic performance acceptance tests – Grades 1 and 2. The pump performance curve is measured with accuracy according to Grade 2 and the medium of fluid used is clean cold water. Flow rate, pump head, net positive suction head, pump speed and power are measured to plot the pump performance curve.

The pump is tested in standard configuration with pressure transmitters are used at suction and discharge section to measure the pump head across the pump. The pressure transmitters are located two diameters upstream of the suction flange and two diameters downstream of the discharge flange respectively. The pressure transmitter used is Endress and Hauser Cerebar PMC 731 model. The measurement range of the suction pressure transmitter is -100 to 200 KPa while the discharge pressure transmitter is -0.1 to 4 MPa. The volume flow rate is measured by a magnetic flow meter, Danfoss MAGFLO MAG3100 series at the downstream of pump and is controlled by a control valve. The accuracy of the magnetic flow meter is 0.25% of the reading and with an output signal of 0~10KHz.

The power is measured by using an Ampere Meter, a Volt Meter and a Power Factor Meter. To measure the pump speed, a magnetic sensor is attached to the pump shaft coupling. An in house designed program is used to collect all the test parameters, as well as to calculate and plot the pump characteristic curve.

3. Numerical Model

In this centrifugal pump numerical computation analysis, a commercially available CFD code, CFX 11.0 has been used to study the complex three-dimensional turbulent flow through the pump at design point. CFX 11.0 is a general purpose CFD code solving three dimensional Reynolds Averaged Navies-Stokes (RANS) equation for steady and turbulent fluid flow. Many researchers have used this CFD code for numerical computation. Satisfactory and good agreements between the numerical and experimental results have been obtained. Asuaje et al [13] performed a quasi-unsteady flow simulation for a centrifugal pump by using the same software. The numerical and test results of the pressure fluctuation at impeller exit are globally satisfactory. Feng et al [14,15] compared the CFD results well with the PIV and LDV results qualitatively and quantitatively at different operating points. Hence with the above validations of the commercial CFD code by other researchers, it could relatively assure that the CFD code can give a reasonable accuracy compare with the experimental results.

In this work, the standard k-ε turbulence model is used and the walls are modeled using a log-law wall function. For the numerical simulation, an unstructured tetrahedral meshing for all the computational domains is used. The reason of using unstructured mesh in current analysis is due to the complexity and irregular profile of the intake section, impeller and volute geometry. The meshes of three computational domains, the intake section, impeller and volute casing, are generated separately. The computational domains at the inlet of intake section and outlet of volute section are extended to allow recirculation. The extension is equal to two times of intake inlet and volute outlet diameter, which is the same as the actual pressure measurement location in the test rig. A localized refinement of mesh is employed at regions close to volute tongue area, impeller blade leading and trailing edge in order to accurately capture the flow field structure. This is because the flow field properties variation such as pressure and velocity at these regions are expected to be substantial.

Figures 1 and 2 show the mesh assembly of intake, impeller and volute sections. The number of elements used in the numerical simulation is fixed after the mesh independence study. In this case, the impeller, volute casing and intake section are meshed with 151866, 114045 and 61211 nodes respectively.

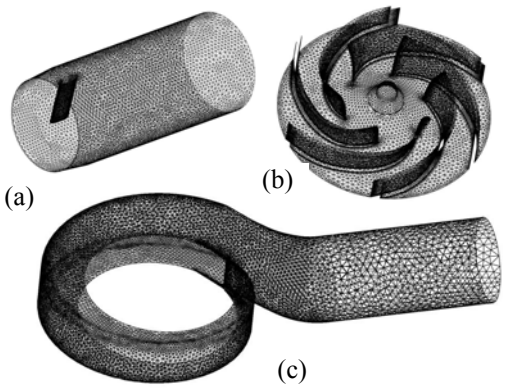

Fig. 1 Mesh model of (a) straight intake section (b) impeller, and (c) volute casing.

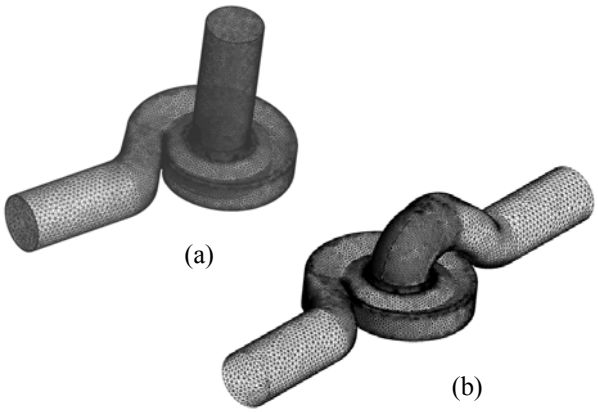

Fig. 2 Mesh model of (a) straight intake section and (b) curved intake section pumps.

3.1 Steady Flow Computation and Boundary conditions

The steady numerical computation is carried out with a multiple frames of reference (MFR) approach because the impeller flow field is with reference to a rotating frame whereby the volute casing and intake section refer to a stationary frame. The dissimilar meshes of the tetrahedral elements of intake section, impeller and volute that generated separately are connected by means of a "Frozen-Rotor" interface. For this kind of interface, the flow field variation across the interface is preserved. For steady calculations the relative position between impeller and volute casing modeled in the inter frames of reference is fixed in time and space. In this case, this Frozen-Rotor interface transfers the non axis-symmetric flow distribution developed only at the given relative position between the impeller and the stationary components to the neighboring region. Any circumferential flow distribution change due to the variation of the relative position between the impeller and volute casing is not considered in this interface. Although Frozen-Rotor interface is mainly used for the axis-symmetric flow problem, but the fast convergence of this model can save large computational time to obtain the overall pump performance curve. The numerical computation is considered converged when the maximum residual 10^{-4} is reached

For the boundary conditions in this study, the absolute inlet pressure and turbulent intensity of 5% are specified because the pressure measurement at the inlet is a known value. The volute casing and intake section walls are in stationary frame and modeled using a no-slip boundary condition. A scalable wall function is applied. In the simulation, the different mass flow rate at the outlet is specified. However, due to strong recirculation and backflow at the outlet, there will be convergence difficulties if the volute outlet section is not extended.

4. Results and Discussion

Prior to any discussion of the unsteady flow field developed in the pump, a comparison of the numerical and experimental performance curves for the curved and straight intake section pumps are shown in Fig. 3. The numerical global characteristics curves obtained are based on the steady computation. The numerically predicted pump characteristic curves over a wide flow range is in good agreement with the experimental results for both curved and straight intake section pumps. The numerical predicted head coefficient ψ is slightly lower than the experimental value but the numerical prediction of the pump efficiency η is slightly higher than experimental value.

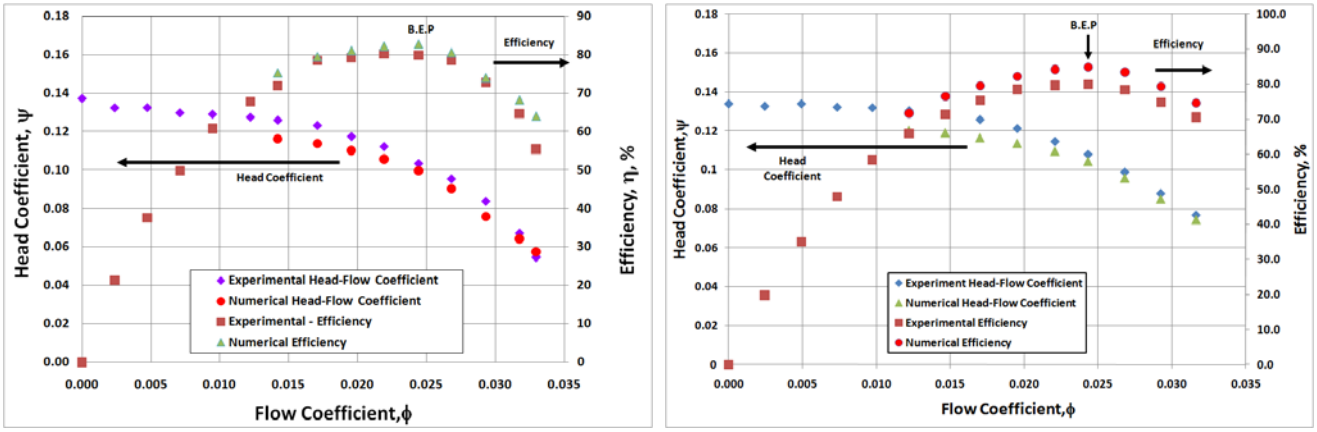

(a) Curved intake section pump (b) Straight intake section pump

Fig. 3 Experimental and numerical comparison of pump performance

For curved intake pump, the numerical predicted ψ is 0.099 as compared to the experimental ψ of 0.103, with a difference of about 4% at the best efficiency point with ϕ of 0.024. At higher flow rate, 130% of Q_{design}, or with ϕ of 0.032, the numerical ψ is 0.064 as compared to experimental ψ of 0.067, which is 5 % difference. However, at lower flow rate condition, 70% Q_{design}, or ϕ of 0.017, the numerical ψ is 0.114 as compared to experimental ψ of 0.123, which is about 7.3% lower. For straight intake section

pump, similar accuracy of numerical result is obtained as well. At best efficiency point with ϕ of 0.024, the numerical predicted ψ is 0.104 as compared to experimental ψ 0.108, with a different of 3.7 %. At 130% Q_{design},or ϕ of 0.032 the numerical ψ is 0.074 as compared experimental ψ of 0.077, which is 3.9% difference. However, at part load condition, 70% Q_{design},or ϕ of 0.017 the numerical predicted ψ is 0.117 as compared to experimental ψ of 0.126, which is about 7.1% lower. Even though both pumps have similar efficiency, but the head coefficient of curved intake section pump is lower than the straight intake section pump at the same flow coefficient ϕ. For curved and straight intake section pump, the head coefficients ψ are 0.103 and 0.108 respectively with the same flow coefficient ϕ of 0.024.

The curved and straight intake section pumps numerical predicted efficiency is 82.71% and 85.87% respectively. However, the actual pumps best efficiencies are at 79.86 % and 79.93 % only. In both cases, the numerical predicted efficiency are higher that experimental one. This is because the numerical predicted efficiency only considered the torque within the rotating impeller without considering mechanical and leakage losses arise in the actual pump model. When modeling the centrifugal pump without side spaces and leakage path, the numerical torque is lower than measured shaft torque and this will increase the numerical efficiency of the centrifugal pump. If disk frictional and leakage losses are included, good agreement between numerical and experimental will be able to achieve.

5. Secondary flow structures at intake section

In order to visualize how the pre-rotation or pre-swirl flow developed upstream before impeller eye for the straight intake section pump, Figs. 4 and 5 show how the velocity and pressure contour changes according to flow rate. In Fig. 4(a) at $0.7Q_{design}$, it is observed that the pre-swirl flow is developed near the right top corner of the intake section but block by the swirl breaker. Thus, a low flow zone is formed behind the vane. Fig 5 (a) shows the pressure contour at $0.7Q_{design}$ with high pressure zone concentrated at the low flow region. When the pump is running at best efficiency point, the more uniform flow velocity and pressure contour observed in Fig. 4 (b) and Fig. 5 (b). It is well known that at design flow rate, the flow has zero incidence flow angle and tangent to the blade leading edge. As expected, at higher flow rate at $1.3Q_{design}$, the pre-swirling flow is developed at the left top corner of the intake. However, the flow behind the vane is not totally stalled as what has seen in the low flow case. In fact, there is a continuous flow velocity contour. This suggested that at higher flow rate, the pre-swirling flow has higher momentum the interaction with the impeller eye is stronger.

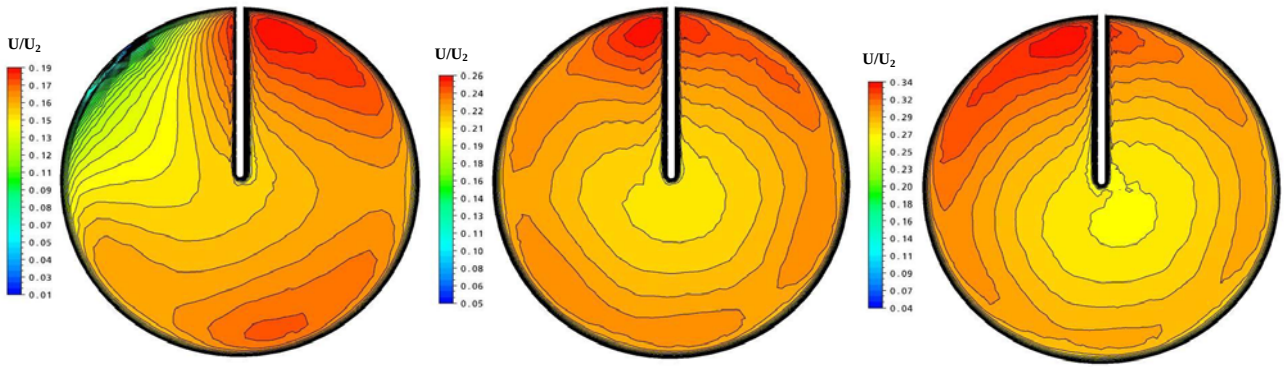

(a) 0.7 Q_{design} (b) Q_{design} (c) $1.3Q_{design}$

Fig. 4 Velocity contour at straight intake section at different flow rates.

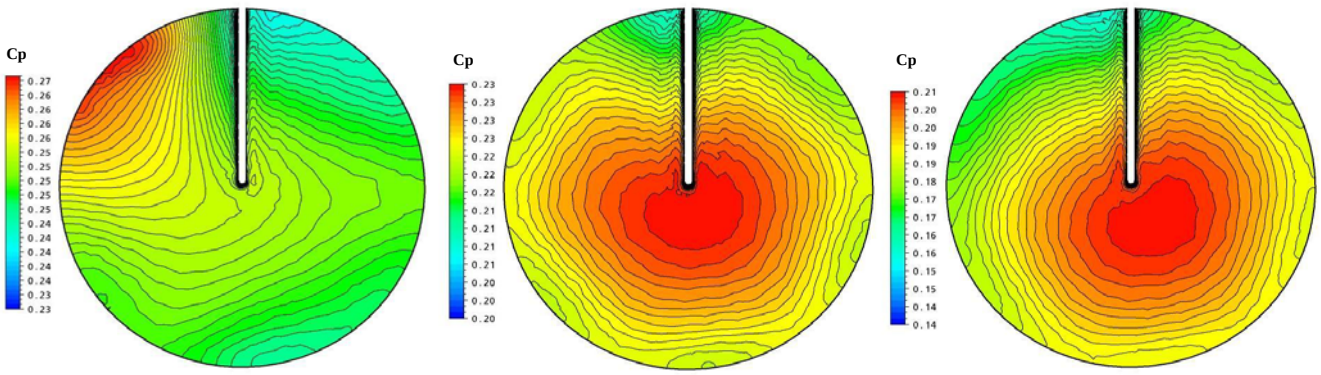

(a) 0.7 Q_{design} (b) Q_{design} (c) $1.3Q_{design}$

Fig. 5 Pressure contour at straight intake section at different flow rates.

Figure 6 shows the cross-section view of the curved intake section. The curved intake section is designed in such a way that it has a non-circular but constant cross-sectional area. The inlet section connecting to upstream pipe is circular and progressively change to a corner-rounded rectangle section at mid-span and becomes circular again just before the impeller eye. A straight partition vane is located at the middle intake section before the impeller eye and is shown as dotted line in Fig 6. The distance

from the center of the impeller to the intake section just before two times of intake diameter extension, L, is 500 mm. The dimensionless distances of plane P1 to P3, x/L, to the center of the impeller are 0.24, 0.38 and 0.5 respectively. After plane P3, the planes P4 to P8 are advancing in angular direction with an increment 18 degree with reference to the centre of the curvature.

According to free vortex flow theory in a curved pipe flow, the pressure increases radially outward from the centre of curvature while the velocity decreases, as described by:

$$\frac{dp}{dr} = \rho \frac{V^2}{r} \tag{1}$$

where p is the pressure, r is the radius of curvature and V is velocity along the curved path. Often, flow separation is occurred at the inner wall and spiraling cross flow motion is appeared in the centre of the pipe towards the outer wall.

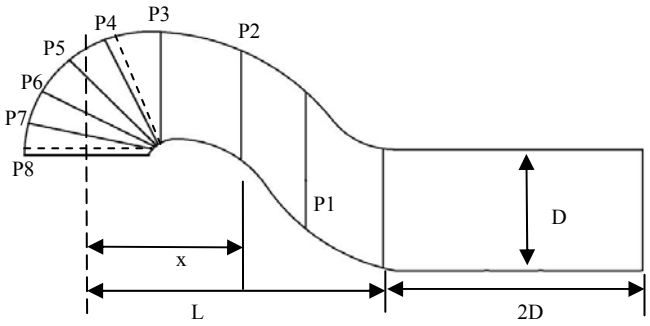

Fig. 6 Cross sectional view of curved intake section.

Figures 7 and 8 show the two-dimensional streamline flow and pressure contour plot along the curved intake section at different plane as shown in Fig 6. At design point, starting from plane P1, the flow is very smooth, not yet influenced by the bend but the flow at top wall region becomes unstable and starts separating. At plane P2, the fluid near the outer wall is decelerated due to change of pressure gradient and the curvature effect starts to influence the main flow to cause a secondary flow forming on the top wall region.

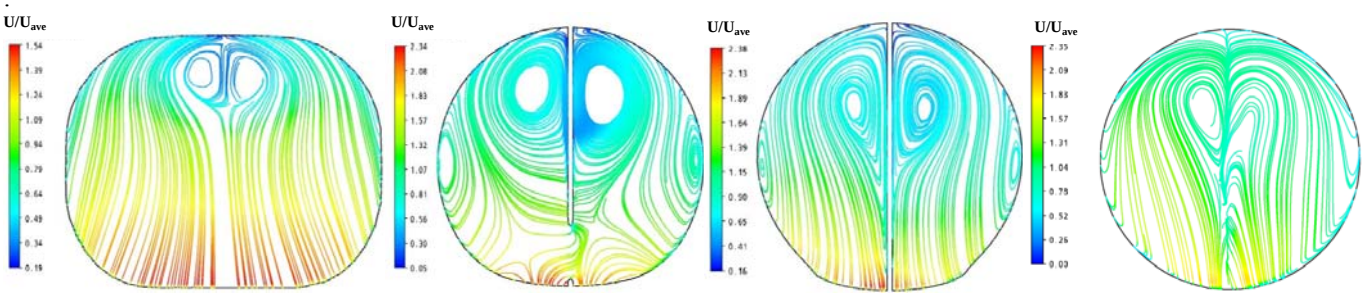

(a) P 2 (b) P4 (c) P 6 (d) P8

Fig. 7 2D streamline at different location along the curved intake section.

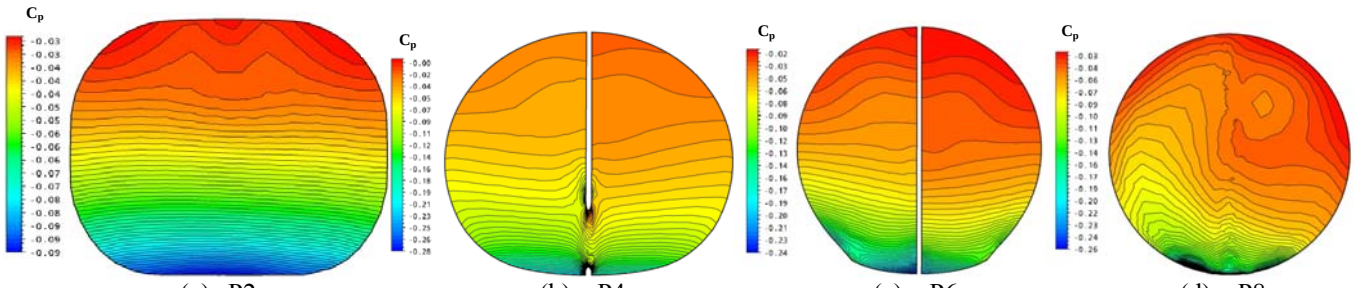

(a) P2 (b) P4 (c) P6 (d) P8

Fig. 8 Pressure contour at different location along the curved intake section

Further downstream at plane P3 (not shown here), the secondary flow due to the centrifugal force appears in the cross and grows up rapidly, forming two counter rotating vortices that circulate outwards in the top central part of the curved pipe and inwards near the left and right walls.

At plane P4, where the partition vane starts dividing the main flow, the fluid near the inner bend is accelerated by the secondary flow. The results show the development of strong pressure-driven secondary flows in the form of a pair of counter-rotating vortices in the stream wise direction. Asymmetrical flow observed near the lower part of the partition vane. This because the flow at impeller eye is started interacting with flow main flow entering it. The slower fluid near the outer wall continues in circular motion towards the top wall. It is observed that another secondary counter rotating vortex flow on the side walls. The formation of the side wall vortex is originated from the plane P3, where spiraling flow is started.

Further downstream at plane P6, the two pair of counter rotating vortices are being suppressed by the momentum of fast moving fluid. The core of the main vortex is shifted to the closer center of the bend while the secondary vortex core is pushed to

the side walls. However, these secondary vortex core flow within a circular cross section are not reported by the measurements of water flows obtained using laser doppler velocimetry by Enayet et al. [16] and Azzola et al. [17].

As noticed in plane P8, the asymmetrical vortical flow structure will propagate further downstream to impeller eye. This results in greatly distorted velocity contours. Because of this secondary flow, the flow into the impeller eye cannot be assumed to be shock-less entry any more. Therefore, shock loss is increases and reduces the pump head generated for curved intake section pump.

However, at off-design point, with $0.7Q_{design}$ and $1.3Q_{design}$, no significant flow structure difference from the design point. This is because of the straight partition vane placed in the curved intake section. Based on what has discussed, it can be concluded that the inlet distortion developed upstream of the impeller eye can caused incorrect incidence and circumferentially distorted patterns in the impeller passage.

6. Impeller volute casing interaction

Figure 9 shows the velocity vector at mid-span of the impeller passage as well. When the centrifugal pump is running with 0.7 Q_{design} , a strong recirculation flow developed on the blade suction towards downstream of the passage. On the pressure side, the flow is attached on the blade and follows the curvature the blade well. This phenomenon could be considered as jet-wake structure development phase as reported by many researchers. The jet-wake structure is found to be caused from leading edge flow separation on suction side.

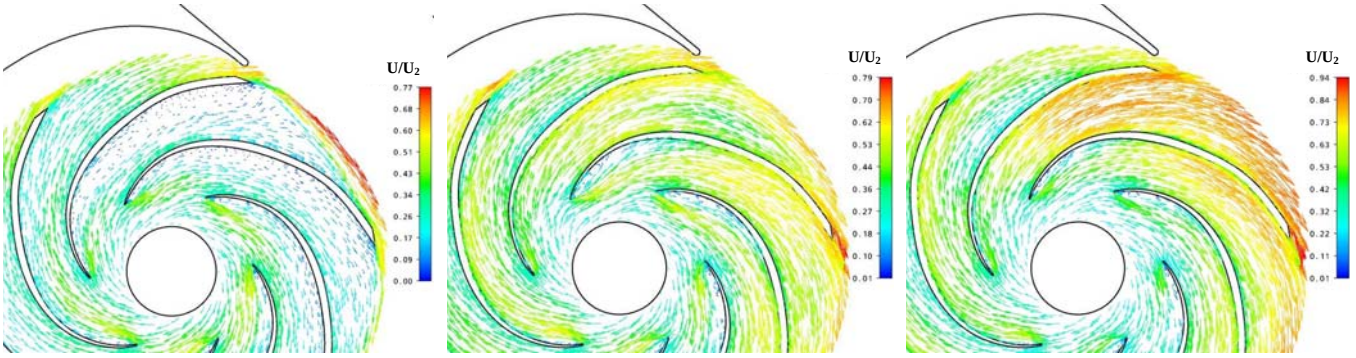

(a) $0.7Q_{design}$ (b) Q_{design} (c) $1.3Q_{design}$

Fig. 9 Velocity vector at mid span of the impeller passage at various flow rates.

At Q_{design}, the velocity vector inside impeller passage also very smooth and leading edge recirculation of flow is observed on the suction side but diminishing towards downstream of the impeller passage. The leading edge separation could stretch up to 15% of the blade cord length downstream. As pointed out previously, the flow into the pump is strongly influence by the secondary flow developed upstream in intake section. This leading edge separation could lead to energy loss in the pump and could further influence the flow field in impeller passage in stream wise direction.

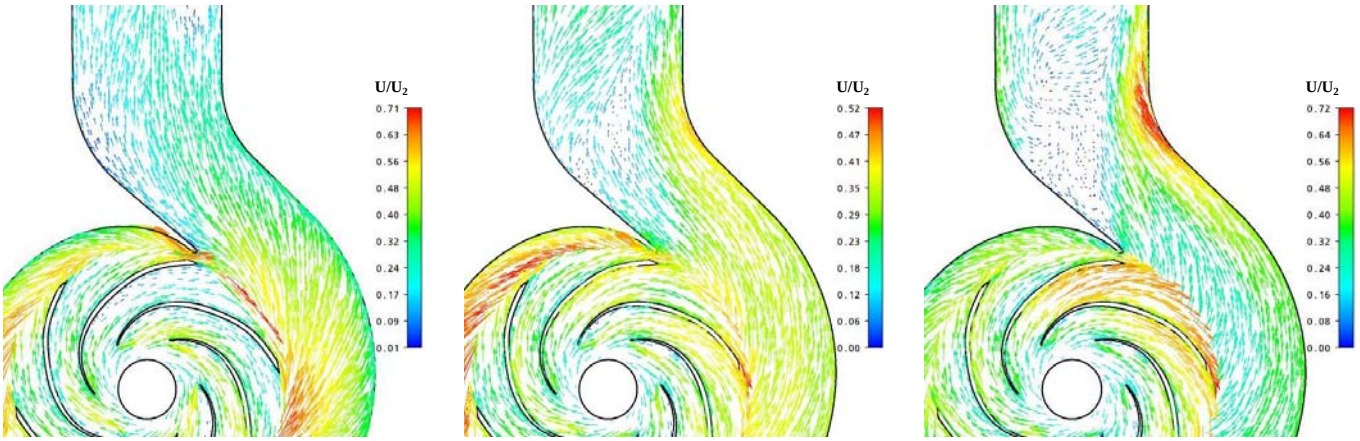

(a) $0.7Q_{design}$ (b) Q_{design} (c) $1.3Q_{design}$

Fig. 10 Velocity vector at near volute tongue and exit at different flow rates.

At $1.3Q_{design}$, the flow within the impeller passage follows the blade curvature very well but the leading edge flow recirculation is less as compared to Q_{design}. As pointed previously, the pre-rotation developed in intake section is flow rate dependent. At higher flow rate, the pre-rotation is opposing the rotation direction of the impeller and incidence angle on the blade leading edge should be positive, on the blade pressure side.

As observed by Elhom and Alder [18] in the flow visualization, the incidence angle of the flow towards volute tongue is flow rate dependent. At optimum flow rate, zero incidence flow angle observed. At high flow rate, a high positive flow incidence angle and with low flow, negative flow incidence angle at volute tongue. Fig. 10 shows the flow pattern at the mid impeller span, z/b=0.5 at volute outlet with different flow rate. At Q_{design}, the flow collected in the volute casing flowing out smoothly at volute diffuser section. However, there is still a secondary flow observed at the mid section of the volute exit plane.

As compared to lower flow rate, even with lack of momentum, a near zero incidence flow angle at volute tongue is observed.

Based on this observation, it is suggested that this flow rate is may be optimum for this particular volute casing tongue angle design. At $1.3Q_{design}$, a significant backflow is re-entering impeller passage through volute tongue and flow is blocked and stalled at the back of volute tongue because of the positive incidence flow angle.

Due to the spiraling geometry of the volute casing and position of the tongue, the flow discharged from the impeller is unmatched. Because of this, it is expected that the radial force will be unbalanced at various operating conditions. Stepanoff [19] showed that the pressure distribution around the volute casing is flow rate dependent. This is further confirmed by the measurement done by Iversen et al [20] about static pressure difference across volute wall in circumferential direction.

Figure 11 shows the pressure distribution within the impeller and volute casing at various flow rates. The pressure increases gradually along stream-wise direction within impeller blade-to-blade passage and has higher pressure on pressure surface than suction surface for each passage. The pressure contour isobar lines are not all perpendicular to the pressure side of the blade inside the impeller passage especially near the leading edge due to the flow separation as mentioned above. The static pressure on the casing also indicated that there is a pressure change from lower flow rate to higher flow rate. At low flow rate, more positive pressure is observed near the volute outlet and a uniform pressure around the volute casing at Q_{design}. At higher flow rate, higher pressure around the volute casing rather than the volute exit. From the pressure contour plot, it can be seen how the pressure loading changing according to flow rate and this will in turn affect the blade loading and radial thrust on the impeller.

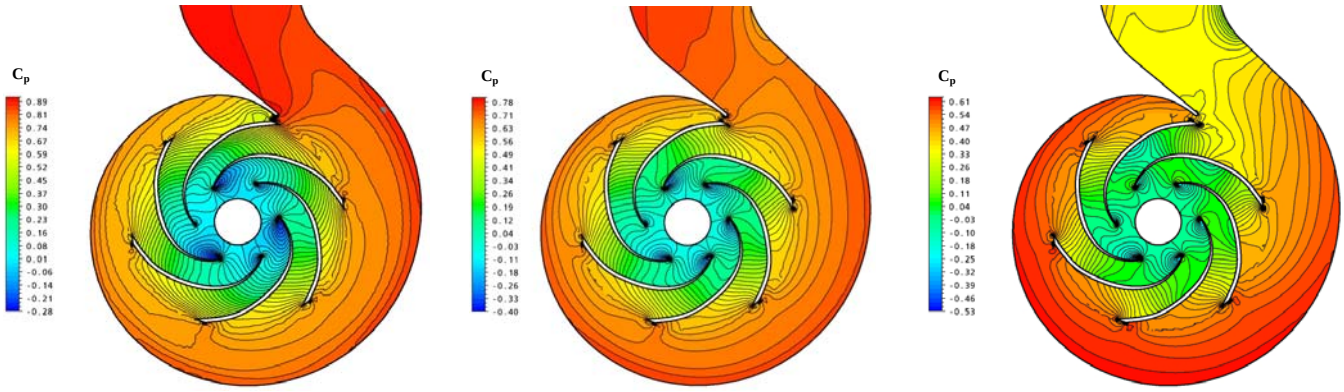

(a) $0.7Q_{design}$ (b) Q_{design} (c) $1.3Q_{design}$

Fig. 11 Pressure distribution around the volute casing at different flow rates.

7. Conclusion

The experimental results show that there is an entrance loss at the curved intake section pump as compared to straight intake section pump. The head coefficient of the curved intake section pump is lower than the straight intake pump even for the given same flow coefficient.

The numerical computation further confirmed that there are secondary flow structures developed at the upstream inside the intake section before entering the impeller eye. The secondary flow structures developed in the straight intake section is flow rate dependent. At design flow rate, an uniform flow is developed. However, at higher or lower flow rates, pre-rotation flow developed upstream in either opposing or following the rotation of the impeller. For curved intake section, because of the radius of curvature, counter-rotating vortex developed upstream has great influence on the head coefficient of the pump.

Strong impeller and volute casing interaction have been investigated as well. The flow within the impeller passage is flow rate dependent and jet wake flow pattern is found at lower flow rate. As the flow discharge from impeller into the volute casing, strong recirculation flow behind the volute tongue is observed due to the incidence angle at volute tongue. Because of the volute position and location, the pressure distributions around the volute casing also strongly dependent on the flow rates.

Nomenclature

A	Cross-sectional Area [m^2]	Q	Volume flow rate [m^3/s]
b_2	Impeller outlet width [m]	r	Radius, radius of curvature [m]
c_p	Pressure coefficient(=$p-p_{atm}/ 0.5\rho U_2^2$)	U	Velocity [m/s]
d_1	Impeller outlet diameter [m]	U_{ave}	Mean velocity(=Q/A)
d_2	Impeller outlet diameter [m]	U_2	Blade tip velocity (=ωr)
g	Gravity acceleration [m^2/s]	Re	Reynolds number (=$u_2 d_2/\nu$)
H	Pump head [m]	n_s	Specific speed (=$N\sqrt{Q} / (gH)^{3/4}$)
N	Rotation speed [rad/s]	ν	Kinematic viscosity
p	Pressure	ψ	Non-dimensional head coefficient (=$gH/N^2d_2^2$)
		ϕ	Flow coefficient, (=Q/Nd^3)

References

[1] Predin, A. and Biluŝ I., 2003, "Influence of Additional Inlet Flow on the Prerotation and Performance of Centrifugal Impellers," J. of Hydraulic Research, Vol. 41, No. 2, pp. 207-216.

[2] Bolpaire S., Barrand J.P., and Caignaert G., 2002, "Experimental study of the flow in the suction pipe of a centrifugal impeller:

steady conditions compared with fast start-up," International Journal of Rotating Machinery, 8(3):215-222.
[3] Kikuyama K., Hasegawa H., and Maeda T., 1992, "Unsteady Pressure Change in Centrifugal Pump Impeller Passages due to Inlet Swirl," J. of Fluids and Structures, Vol. 6, pp. 337-351.
[4] Bwalya A.C. and Johnson M.W., 1996, "Experimental Measurements In A Centrifugal Pump," ASME J. of Fluids Eng., Vol. 116, pp. 692-697.
[5]Howard J.H.G. and Kittmer C.W., 1975, "Measured Passage Velocities in a Radial Impeller with Shrouded and Unshrouded Configurations," ASME J. of Engineering for Power, pp. 207-213.
[6] Murakami M., Kikuyama K., and Asakura, 1980, "Velocity and Pressure distributions in the impeller passages of centrifugal pump," ASME J. of Fluids Eng., 102, pp. 420-426.
[7] Hong S.S. and Kang S.H., 2002, "Exit Flow Measurement of a Centrifugal Pump Impeller," KSME International Journal, Vol. 16, No. 9, pp. 1147-1155.
[8] Pedersen N., Larsen P.S. and Jacobsen C.B., 2003, "Flow in a Centrifugal Pump at Design and Off-Design Conditions – Part I: Particle Image Velocimetry (PIV) and Laser Doppler Velocimetry (LDV) Measurement," ASME J. of Fluids Eng., Vol. 125, pp. 61-72.
[9] Liu C.H., Vafidis C., and Whitelaw J.H., 1994, "Flow Characteristics of a Centrifugal Pump," ASME J. of Fluids Eng., Vol. 116, pp. 303-309
[10] Abramian M. and Howard J.H.G., 1994, "Experimental Investigation of the Steady and Unsteady Relative Flow in a Model Centrifugal Impeller Passage," ASME J. of Fluids Eng., Vol. 116, pp. 269-279.
[11]Dong R., Chu S., and Katz J., 1992, "Quantitative Visualization of the Flow Within the Volute of a Centrifugal Pump. Part B: Results and Analysis," ASME J. of Fluids Eng., Vol. 114, pp. 396-403.
[12] Chu S., Dong R., and Katz J., 1995, "Relationship Between Unsteady Flow, Pressure Fluctuations, and Noise in a Centrifugal Pump; Part B: Effects of Blade-Tongue Interactions," ASME J. of Fluids Eng., Vol. 177, pp. 30-35.
[13] Asuaje M., Bakir F., Kergourlay G., Noguera R., and Rey R., 2006, "Three-dimensional Quasi-steady Flow Simulation in a Centrifugal Pump: Comparison with Experiment Results," Proc. IMechE Part A: J. Power and Energy, Vol. 220, pp. 239-256.
[14] Feng J.J., Benra F.K., and Dohmen H.J., 2007, "Numerical Investigation on Pressure Fluctuations for Different Configurations of Vaned Diffuser Pumps," International J. of Rotating Machinery, Vol. 2007, Article ID 34752.
[15] Feng J.J., Benra F.K., and Dohmen H.J., 2009, "Comparison of Periodic Flow Fields in a Radial Pump among CFD, PIV, and LDV Results," International J. of Rotating Machinery, Vol. 2009, Article ID 410838.
[16] Enayet M. M., Gibson M. M., Taylor A. M. K. P., and Yianneskis M., 1982, "Laser-Doppler measurements of laminar and turbulent flow in a pipe bend," Vol. 3, No. 4, pp. 213-219.
[17] Azzola J., Humphrey J.A.C., Iacovides H., and Launder B.E., 1986, "Developing Turbulent Flow in a U-Bend of Circular Cross-Section: Measurement and Computation," ASME J. of Fluids Eng., Vol. 108, pp. 214-221.
[18] Elholm T., Ayder E., and Van den Braembussche R.A., 1992, "Experimental Study of the Swirling Flow in Volute of Centrifugal Pump," ASME J. of Turbomachinery, Vol. 114, pp. 366-372
[19] Stepanoff A.J., 1957, "Centrifugal and Axial Flow Pumps: Theory, Design and Application," 2nd Ed. Krieger, Melbourne, FL.
[20] Iversen H.W., Rolling R.E., and Carlson J.J., 1960, "Volute Pressure Distribution, Radial Force on the Impeller, and Volute Mixing Losses of a Radial Flow Centrifugal Pump," ASME J. of Eng. For Power, pp. 136-144.